archives
of thermodynamics
Vol. **44**(2023), No. 2, 3–20
DOI: 10.24425/ather.2023.146556

Effect of D-shaped, reverse D-shaped and U-shaped turbulators in solar air heater on thermo-hydraulic performance

ABHISHEK GHILDYAL[a]
VIJAY SINGH BISHT[a]
PRABHAKAR BHANDARI[b*]
KAMAL SINGH RAWAT[c]

[a] Veer Madho Singh Bhandari Uttarakhand Technical University, Faculty of Technology, Dehradun 248007, India

[b] K.R. Mangalam University, School of Engineering and Technology, Department of Mechanical Engineering, Gurugram, Haryana 122103, India

[c] Meerut Institute of Engineering and Technology, Mechanical Engineering Department, Meerut 250005, India

Abstract As the cost of fuel rises, designing efficient solar air heaters (SAH) becomes increasingly important. By artificially roughening the absorber plate, solar air heaters' performance can be augmented. Turbulators in different forms like ribs, delta winglets, vortex generators, etc. have been introduced to create local wall turbulence or for vortex generation. In the present work, a numerical investigation on a solar air heater has been conducted to examine the effect of three distinct turbulators (namely D-shaped, reverse D- and U-shaped) on the SAH thermo-hydraulic performance. The simulation has been carried out using the computational fluid dynamics, an advanced and modern simulation technique for Reynolds numbers ranging from 4000 to 18000 (turbulent airflow). For the purpose of comparison, constant ratios of turbulator height/hydraulic diameter and pitch/turbulator height, of 0.021 and 14.28, respectively, were adopted for all SAH configurations. Furthermore, the fluid flow has also been analyzed using turbulence kinetic energy and velocity contours. It was observed that the U-shaped turbulator has the highest value of Nusselt number followed by D-shaped

*Corresponding Author. Email: prabhakar.bhandari40@gmail.com

and reverse D-shaped turbulators. However, in terms of friction factor, the D-shaped configuration has the highest value followed by reverse D-shaped and U-shaped geometries. It can be concluded that among all SAH configurations considered, the U-shaped has outperformed in terms of thermo-hydraulic performance factor.

Keywords: CFD; Renewable energy; Solar air heater; Turbulence kinetic energy; Thermo-hydraulic performance

Nomenclature

A_P	–	heat transfer area, mm^2
C_p	–	specific heat capacity, J/(kgK)
D_h	–	hydraulic diameter, mm
e	–	rib height, mm
fr	–	friction factor
h	–	heat transfer coefficient, W/m^{2}K
H	–	duct height, mm
I	–	heat flux, W/m^2
k	–	thermal conductivity, W/(m K)
l	–	duct length, mm
$\dot{m}$	–	mass flow rate, kg/s
Nu	–	Nusselt number
Pi	–	pitch, mm
p	–	pressure, Pa
Δp	–	pressure drop, Pa
Re	–	Reynolds number
$\dot{Q}_u$	–	useful heat gain, W
T	–	temperature, K
U	–	mean airflow velocity in the duct, m/s
u_i	–	air flow velocity component in i direction ($i = 1, 2$)
W	–	duct width, mm

Greek symbols

ρ	–	density, kg/m^3
μ	–	dynamic viscosity, Ns/m^2
λ	–	thermal diffusivity, m^2/s
v	–	kinematic viscosity, m^2/s

Subscripts

in	–	inlet
F	–	fluid
out	–	outlet
P	–	absorber plate
t	–	solar air heater with turbulator
s	–	smooth solar air heater

Abbreviations

SAH	–	solar air heater
SST	–	shear stress transport
CFD	–	computational fluid dynamics
ASHRAE	–	American Society of Heating, Refrigerating and Air-Conditioning Engineers
THPF	–	thermo-hydraulic performance factor
RNG	–	renormalization group

1 Introduction

The majority of energy is mainly produced using traditional energy sources such as coal, oil, and natural gas. As a result, traditional energy sources are decreasing at an alarming rate. Furthermore, these energy sources also pollute the environment significantly. So, in order to meet the energy needs of such a vast population, some non-traditional energy sources are needed that do not affect the environment and are easily available. As a result, the usage of alternative energy sources such as solar, wind, biomass, and hydropower has been explored very much in recent decades. Major sources are primarily derived from solar energy either directly or indirectly. Solar energy has been used for a variety of applications, including water heating and cooling, space heating, water purification, cooking, and power generation [1–3]. One of the most common uses of solar energy is room heating via a device known as a solar air heater (SAH). SAH is a better device in terms of handiness, maintenance, and environmental damage. However, one of the major drawbacks of SAH is its poor thermal performance, which is caused by a low heat transfer rate from the absorber plate to the fluid flow, i.e. air. Generally, the flow in SAH is in a turbulent regime as more flow has to take place. So, when air molecules collide with a stationary surface, a thin viscous sublayer forms near the wall in turbulent boundary layers, where the damping impact of molecular viscosity on turbulent velocity fluctuation is dominant, as indicated by Bopche *et al.* [4]. Because of the comparatively low velocity of the air and reduced thermal conductivity, the heat transfer rate between the absorber plate and the air in this viscous sublayer is adversely affected. However, artificial roughness, such as baffles and ribs, twisted tapes, dimples, etc. can be used to overcome this problem [5–8]. This roughness causes turbulence inside the air duct,

which causes the laminar sublayer to break down, increasing the heat transfer coefficient. Artificial roughness, on the other hand, causes friction loss. As a result, turbulence must only be induced in the laminar sublayer, i.e. near the duct surface. Turbulators' applications are not limited to solar air heater but has also been used in other cooling devices such as photovoltaic/thermal collector [9], gas turbine blades [10], and car radiator [11].

Chaube *et al.* [12] studied numerically a solar air heater with ribs having square, rectangle, chamfered, circular, semi-circular, and triangular shapes. They observed that rectangular ribs have yielded the best thermo-hydraulic performance. They also pointed out that the shear stress transport (SST) turbulence model, i.e. SST k-ω model, accurately predicts the experimental value. Karmare *et al.* [13] employed rib grits in a circular, triangular, and square shape with five distinct angles of attack of 54°, 56°, 58°, 60°, and 62°. Their study involved Reynolds numbers ranging from 3600 to 17 000. In the commercial solver (Ansys Fluent), they used the k-epsilon model. They found that a 58° angle of attack has yielded optimum performance. Rajput *et al.* [14] used square, triangular, rectangular, and chamfered turbulators to evaluate flow properties in a SAH. For the analysis, they employed the SST k-ω turbulent model. They observed that triangular and chamfered turbulators provided better thermal characteristics while rectangular turbulators have the best overall performance index among all the configurations. Chaube *et al.* [15] analyzed nine different forms of ribs in a rectangular duct using the SST k-ω model in the CFD program. They found that rectangular ribs with a surface area of 3 mm $\times$ 5 mm had the best performance index. Furthermore, they also pointed out that two-dimensional analysis predicts the experimental results more accurately. Yadav and Bhagoria performed a parametric computational study on a solar air heater having equilateral triangular sectioned rib roughness on the absorber plate [16]. They reported that the thermo-hydraulic performance parameter varies between 1.36 and 2.11 for different geometrical parameters of ribs. Semalty *et al.* [17] employed a novel approach of multiple broken arc and circular protrusions as roughness in a solar air heater and found that such configuration improves the thermal performance of the solar air heater with a minimum penalty of frictional pressure drop. Bohra *et al.* [18] roughened their absorber plate with 45° Z-shaped baffles in their numerical study and found that a blockage ratio of 0.3 yielded optimum performance.

Following the above discussion, we have found that the turbulator shapes can significantly affect the thermo-hydraulic performance of a solar air

heater. So, in the present work, three different shaped turbulators i.e. D-shaped, reverse D-shaped, and U-shaped were studied. They are named according to their constructional feature. As per the best knowledge of the authors, these turbulator configurations have not been reported for solar air heaters and the same is the novelty of the present work. These turbulators were attached to the absorber plate to disturb the viscous sublayer. Furthermore, the investigation was carried out to visualize the impact of variation in Reynolds number on the fluid flow characteristics, heat transfer, and friction. The prime objective of the present work is to explore the possibility of enhancement in the thermo-hydraulic performance of solar air heaters using differently shaped turbulators.

2 Numerical modelling

2.1 Computational domain

Using three various types of turbulators, a two-dimensional numerical analysis was carried out to see how the performance of the solar air heater would change. The schematic diagram of the solar air heater in its operation is shown in Fig. 1a. The geometries of turbulators employed in this study were U-shaped, D-shaped, and reverse D-shaped as depicted in Fig. 1b. In this study, we built the two-dimensional rectangular SAH duct domain in the same way as Chaube *et al.* [15] did. The 2D flow domain was designed using the principles of ASHRAE standard 93-2003 [19]. The use of a numerical approach, i.e. computational fluid dynamics solver, is more common in similar types of problems [20, 22, 23] and predicts the flow physics accurately. The present simulations has been carried out in the CFD commercial code Ansys Fluent V 16.0. The duct is divided into three sections. The input and output sections are 245 and 115 mm, respectively. The length of the test segment is 280 mm. The area where the absorber plate is installed is known as the test section. The absorber plate is where the various turbulators are mounted. On this absorber plate, a continuous heat flux of $I = 1000$ W/m^2 is applied to model the solar radiation. The rib height is kept constant at 0.7 mm and the pitch is kept at 10 mm. The temperature of the working fluid and ambient air at the inlet is 300 K. The hydraulic diameter is estimated to be 33.33 mm. Table 1 summarises the parameters applied in the simulations.

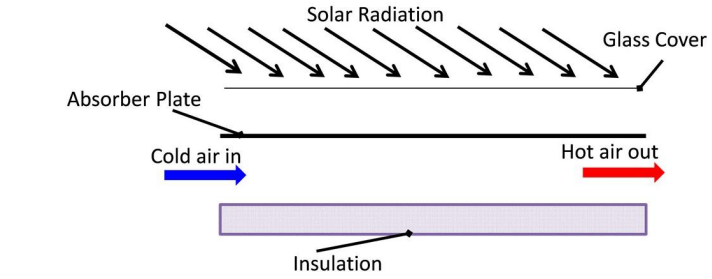

(a)

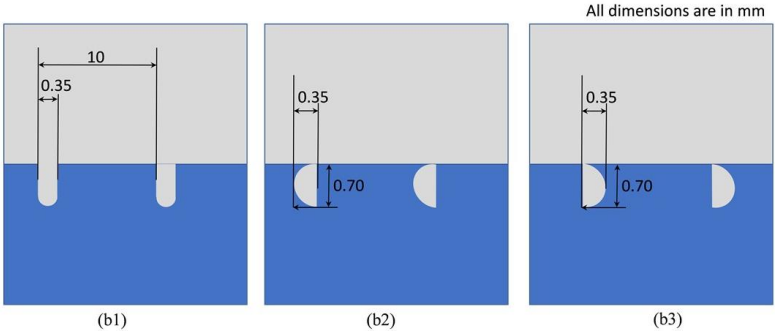

(b)

Figure 1: A diagram of the solar air heater (a) and differently shaped turbulators: U-shaped (b1), reverse D-shaped (b2), and D-shaped (b3).

Table 1: Parameters employed in the analysis.

Parameters	Symbols	Values
Total length of the duct, mm	L	640
Duct width, mm	W	100
Duct height, mm	H	20
Roughness ribs height, mm	E	0.7
Pitch, mm	Pi	10
Hydraulic diameter, mm	D_h	33.33
Relative roughness pitch	Pi/e	14.285
Relative roughness height	e/D_h	0.021
Uniform heat flux, W/m^2	I	1000
Reynolds number	Re	4000, 8000, 12000, 16000, 18000
Inlet temperature of the air, K	T_{in}	300

2.2 Grid generation

The computational domain of SAH has been discretized in quadrilateral structural meshing. Furthermore, to get uniform meshing throughout SAH, face meshing and body sizing of 0.2 mm was used. The meshed image of SAH having D-shaped turbulators is shown in Fig. 2 with a zoomed view. The grid independence test has also been carried out to predict results more accurately in lesser computational time. The grid convergence index (GCI) has been used to measure the relative change in the corresponding magnitude with the grid refinement [24, 25]. However, in the present work, the average Nusselt number for different mesh sizes has been compared. Table 2 highlights the change in the Nusselt number with variation in the number of elements in the computational domain. As the number of elements for the D-shaped configuration increases, the percentage variation of the Nusselt number decreases. Furthermore, it was observed that the mesh size between the last two cases has very low variation, so the number of 319 907 cells was considered in further studies.

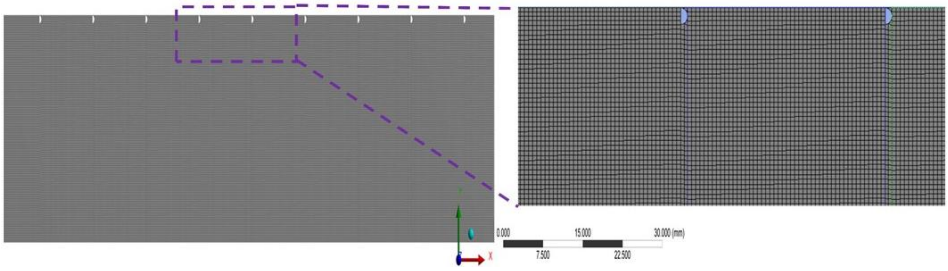

Figure 2: Meshing of SAH having D-shaped turbulators.

Table 2: Grid independence test in SAH with the D-shaped turbulators.

Number of nodes	Number of cells	Nusselt number	Variation, %
280781	100242	66.32	–
564231	201264	92.68	39.74
898165	300127	110.89	19.65
966392	319907	114.59	3.34
1001879	340213	114.74	0.13

2.3 Governing equations

The fluid phenomenon in artificially roughened rectangular solar air heater ducts is solved by using steady-state two-dimensional continuity equation, time-independent incompressible Navier–Stokes equations and the energy equation [5, 17]. These equations can be written in the Cartesian tensor system as follows:

Equations of continuity:

$$\frac{\partial u_i}{\partial x_i} = 0, \quad i = 1,\, 2\,, \tag{1}$$

where x_i are the Cartesian coordinates and u_i are the components of fluid velocity in x_i-direction.

Equations of momentum:

$$\frac{\partial\left(u_i u_j\right)}{\partial x_j} = \frac{1}{\rho}\frac{-\partial p}{\partial x_i} + \frac{\partial\left[\nu\left(\dfrac{\partial u_i}{\partial x_j} + \dfrac{\partial u_j}{\partial x_i}\right)\right]}{\partial x_j} - \frac{\partial\left(\overline{u_i' u_j'}\right)}{\partial x_j}, \quad i, j = 1, 2\,, \tag{2}$$

where p is the pressure, ρ and μ are the density and dynamic viscosity of air, respectively, over-bar denotes a time averaged quantity and prime denotes the deviation from average. The last term on the right-hand side of Eq. (2) is the Reynolds stress tensor and represents the effect of the turbulent fluctuations on the decomposed velocity and pressure fields.

Equation of energy:

$$\frac{\partial}{\partial x_j}\left(u_j T\right) = \frac{\partial}{\partial x_j}\left[\left(\lambda + \lambda_t\right)\frac{\partial T}{\partial x_j}\right], \tag{3}$$

where T is the thermodynamic temperature at different location. The symbols λ and λ_t are molecular thermal diffusivity and turbulent thermal diffusivity, respectively.

Adding turbulators in the fluid flow duct enhances heat transfer, as predicted by calculating Nusselt numbers [26, 27]. In addition to this enhancement, the friction factor also increases. In artificially roughened solar air heaters, the Nusselt number is calculated as follows:

$$\mathrm{Nu} = \frac{hD_h}{k} = \frac{\dot{Q}_u D_h}{A_P\left(T_P - T_F\right)k}, \tag{4}$$

where A_P is the heat transfer area, D_h, k, and h denote the hydraulic diameter of the duct, the thermal conductivity of air, and the heat transfer

coefficient between the air and SAH absorber plate, respectively. Parameters T_P and T_F are the average temperatures of the absorber plate and fluid, respectively. The quantity $\dot{Q}_u$ is the heat gained by air during its flow in the SAH duct and is calculated using the equation

$$\dot{Q}_{\boldsymbol{u}} = \dot{m} C_p \left(T_{\text{out}} - T_{\text{in}}\right), \tag{5}$$

where $\dot{m}$ is the mass flow rate of air in the duct, C_p is the specific heat capacity, T_{out} and T_{in} are temperatures of air at the outlet and inlet cross-sections, respectively.

The friction factor is calculated as

$$fr = \frac{\dfrac{\Delta p}{l} D_h}{\dfrac{1}{2}\rho U^2}, \tag{6}$$

where Δp is the pressure drop across the test section length (l) of an artificially roughened solar air heater and U is the mean velocity of the air i.e. resultant of u_i and u_j. The Reynolds number is calculated as

$$\text{Re} = \frac{\rho U D_h}{\mu}, \tag{7}$$

where μ is the dynamic viscosity of air.

Thermo-hydraulic performance factor (THPF) has been proposed by Webb and Eckert [28] and the expression used in the present work is

$$\text{THPF} = \frac{\dfrac{\text{Nu}_t}{\text{Nu}_s}}{\left(\dfrac{fr_t}{fr_s}\right)^{\frac{1}{3}}}, \tag{8}$$

where subscripts t and s stand for solar air heater duct with and without turbulators, respectively.

2.4 Validation of results

The results of the present numerical model have been validated with the research outcomes of Yadav and Bhagoria [16]. They opted equilateral triangular sectioned rib on the absorber plate of the solar air heater. The geometry, similar to Yadav and Bhagoria [16] has been created and simulated in commercial code Ansys under the constant value of heat flux

(1000 W/m^2) and using RNG k-ε turbulence model. The variation of two different parameters, i.e. Nusselt number (Nu) and friction factor (fr) with respect to Reynolds number (Re) has been compared as illustrated in Fig. 3. It is observed that our numerical model results are similar to those reported by Yadav and Bhagoria [16]. The deviation in Nu value and fr value can be due to assumptions considered in the present simulation like constant thermophysical property of the working fluid, incompressible flow, etc.

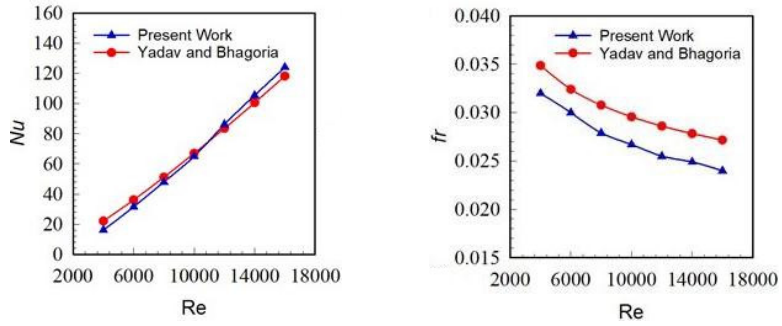

(a) (b)

Figure 3: Comparison of the Nusselt number (a) and friction factor (b) values obtained in the present work with those of Yadav and Bhagoria [16].

3 Results and discussion

The results of the CFD analysis of a roughened solar air heater were thoroughly reviewed. With the help of Ansys Fluent findings, we explored aspects such as heat transfer characteristics, pressure drop, friction factor, turbulent kinetic energy, temperature change, and energy conversion. With the inclusion of different turbulators, the SAH performance varies. Finally, the thermo-hydraulic performance factor is used to compare all three configurations. All simulations were studied under the constant value of relative roughness pitch ($Pi/e = 14.285$) and relative roughness height ($e/D_h = 0.021$).

3.1 Velocity contour

The variation in the velocity of the flowing fluid, i.e. air inside the duct, is depicted in Fig. 4. Furthermore, the figure also shows the zoomed view of the computational domain near the turbulators. The contours have been

plotted for Reynolds number of 18000. The fluctuation in velocity will be reduced if a smooth surface is chosen. However, if some roughness is applied inside the duct, the velocity variation will be greater because the space available for air circulation around the ribs is limited, and the velocity of air should rise below the ribs to maintain a consistent mass flow rate. The turbulence inside the duct will rise as the air velocity increases. This

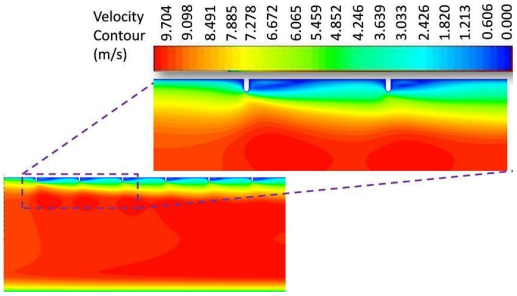

(a)

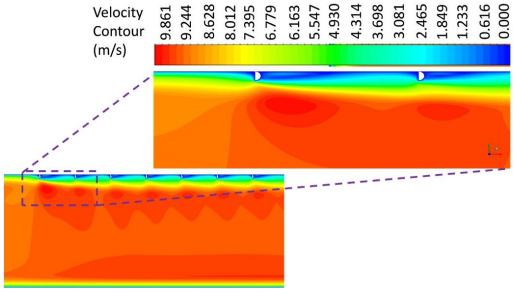

(b)

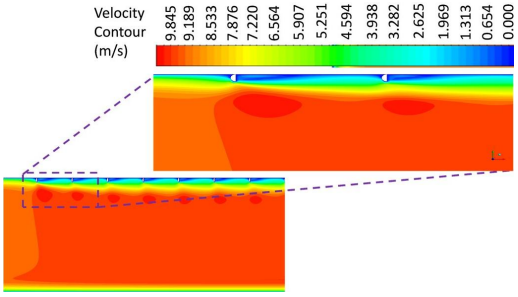

(c)

Figure 4: Velocity contour in the SAH duct employing (a) U-shaped roughness, (b) D-shaped roughness, and (c) reverse D-shaped roughness.

will increase heat transfer between the absorber plate and the air, which is the primary goal of adopting varied roughness. However, there is a penalty, i.e. increase in pressure drop along the flow direction. Due to that more pumping power is required to flow fluid through the duct of SAH.

3.2 Turbulent kinetic energy contour

The mean kinetic energy per unit mass associated with eddies in turbulent flow is known as turbulent kinetic energy. With the help of turbulence kinetic energy, we can directly describe the strength of turbulence in the flow field. The thermal phenomenon in an artificially roughened SAH can be explained using turbulent kinetic energy contours. The contours show that the largest value of turbulent kinetic energy is found near the absorber plate and between the first and second rib and that it decreases along the absorber plate length. The variations of turbulent kinetic energy in SAH for differently shaped turbulators (i.e. U-, D-, and reverse D-shaped) are depicted in Fig. 5.

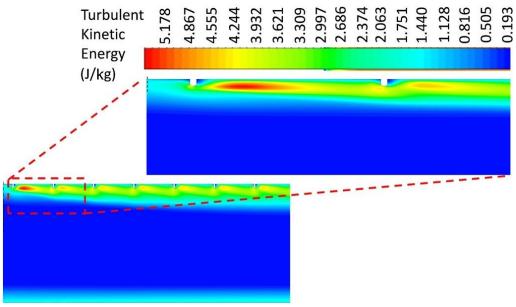

(a)

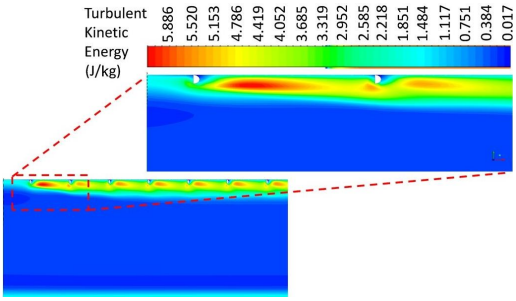

(b)

Figure 5: For caption see next page.

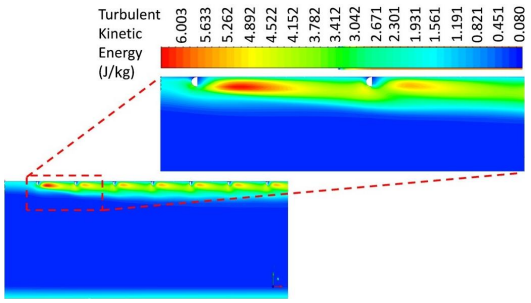

(c)

Figure 5: Turbulent kinetic energy contour in the SAH duct employing (a) U-shaped roughness, (b) D-shaped roughness, and (c) reverse D-shaped roughness.

3.3 Heat transfer and Fluid flow characteristics

A numerical analysis of the solar air heater was carried out in order to determine the heat transfer enhancement. To improve heat transfer, we used three different types of ribs in our investigation. The U-shaped, D-shaped, and reverse D-shaped ribs were considered. All other parameters were maintained constant, hence the properties of the solar heater are mostly determined by the Reynolds number. In this study, the Reynolds numbers ranged from 4000 to 18000. At a Reynolds number of 18000, the maximum heat transfer is obtained. Variation of the Nusselt number with respect to the Reynolds number for all SAH configurations is depicted in Fig. 6. As can

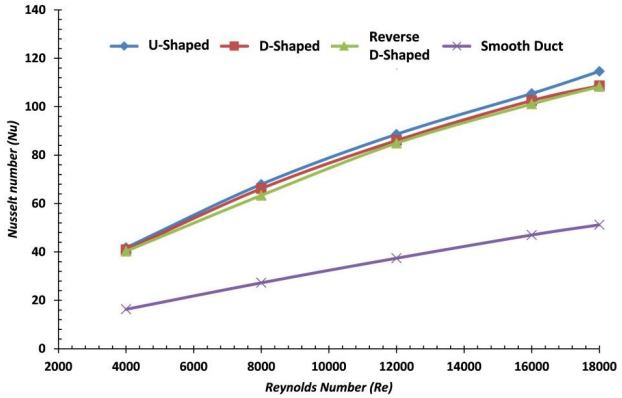

Figure 6: Variation of Nusselt number with Reynolds number for different turbulator geometries.

be seen from the figure, among all configurations U-shaped roughness has shown the best performance.

The change in friction factor with Reynolds number from 4000 to 18000 for all configurations is demonstrated in Fig. 7. As artificial roughness was introduced in the smooth absorber plate, the friction factor increased for all roughened geometries. While among all configurations, U-shaped geometry has shown a minimal friction factor.

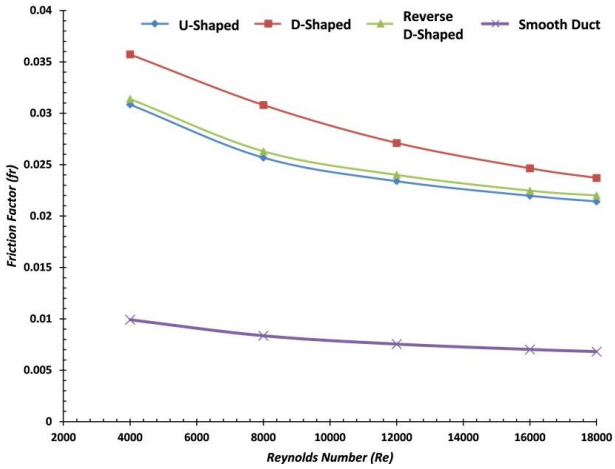

Figure 7: Variation of friction factor with Reynolds number for different turbulator geometries.

3.4 Thermo-hydraulic performance factor

Using different surface roughness in the solar air heater results in enhanced thermal performance but at the expense of pressure drop penalty. Different terms such as the figure of merit, coefficient of performance, thermal performance factor, etc. have been used in the literature to evaluate the design efficacy [29, 30]. The term thermo-hydraulic performance factor has been outlined by Webb and Eckert [28] in the design of the solar air heater and the same has been incorporated here. Obtained results are presented in Fig. 8. They illustrate that among the considered configurations, SAH with U-shaped roughness has the highest value of THPF followed by reverse D-shaped and D-shaped geometries. Furthermore, the THPF value decreases continuously with the Reynolds number due to an exponential increase in pressure drop. The highest THPF of 1.762 was reported for

U-shaped roughness at Re = 4000. There are various optimization techniques like Taguchi [31], Taguchi-Topsis [32], the preference selection index method [33], the hybrid entropy-VIKOR (VIšekriterijumsko KOmpromisno Rangiranje) method [34], the hybrid analytical hierarchy process and preference ranking organization method for enrichment evaluations technique [35], analysis of variance [36], etc., which can be opted in SAH for effective performance.

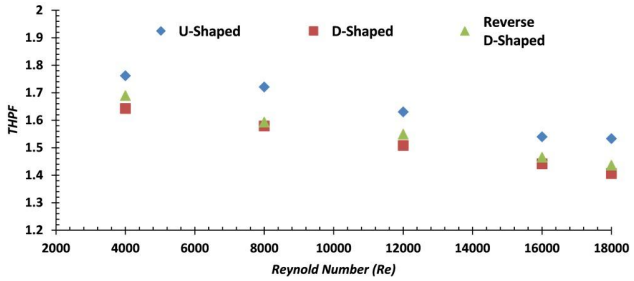

Figure 8: Variation in thermo-hydraulic performance factor as a function of Reynolds number for various geometries.

4 Conclusion

In the present work, a two-dimensional CFD model of a solar air heater having an artificially roughened absorber plate has been analyzed. For comparison purposes, three different roughness shapes, namely D-shaped, reverse D-shaped, and U-shaped were studied for constant turbulator height to hydraulic diameter and pitch to turbulator height ratios of 0.021 and 14.28, respectively. The heat transfer and flow friction characteristics of different roughness shape configurations were compared. The following are the outcomes of the above investigation:

- For the investigation of a two-dimensional rectangular duct, the RNG k-ε model provides satisfactory accuracy.
- For all types of geometry, the Nusselt number increases with an increase in the Reynolds number while the friction factor decreases.
- The presence of turbulators in a solar air heater significantly increases the heat transfer rate but at the expense of an increased friction factor. The maximum enhancement in the Nusselt number was 2.56 times

while the highest friction factor increment was 3.60 times relative to the smooth solar air heater.

- Among different turbulator configurations, the U-shaped configuration has shown the highest value of Nusselt number followed by the D-shaped and reverse D-shaped. In terms of friction factor, the D-shaped configuration had the highest value followed by reverse D-shaped and U-shaped configurations irrespective of Reynolds number.
- Among the examined configurations, SAH with U-shaped turbulators has shown the best thermo-hydraulic performance factor, with the highest value of 1.76 at the Reynolds number of 4000.

Received 2 November 2022

References

[1] Saxena A., Goel V.: *Solar air heaters with thermal heat storages*. Chin. J. Eng. (2013), 4, 90279.

[2] Saxena A., Varun, El-Sebaii A.A.: *A thermodynamic review of solar air heaters*. Renew. Sust. Energ. Rev. **43**(2015), 863–890.

[3] Saxena A., Srivastava G., Tirth V.: *Design and thermal performance evaluation of a novel solar air heater*. Renew. Energ. **77**(2015), 501–511.

[4] Bopche S.B., Tandale M.S.: *Experimental investigations on heat transfer and frictional characteristics of a turbulent or roughened solar air heater duct*. Int. J. Heat Mass Transf. **52**(2009), 2834–2848.

[5] Singh B.P., Bisht V.S., Bhandari P., Rawat K.S.: *Thermo-fluidic modelling of a heat exchanger tube with conical shaped insert having protrusion and dimple roughness*. Aptisi Trans. Technopreneurship (ATT) **3**(2021), 2, 13–29.

[6] Singh B.P., Bisht V.S., Bhandari P.: *Numerical study of heat exchanger having protrusion and dimple roughened conical ring inserts*. In: Advances in Fluid and Thermal Engineering (B.S. Sikarwar, B. Sundén, Q. Wang, Eds.), Lect. Notes Mech. Eng. Springer, 2021, 151–162.

[7] Kharhwal H., Singh S.: *Effect of serrated circular rings on heat transfer augmentation of circular tube heat exchanger*. Arch. Thermodyn. **43**(2022), 2, 129–155.

[8] Kumar V.: *Effect of serrated circular rings on heat transfer augmentation of circular tube heat exchanger*. Arch. Thermodyn. **41**(2020), 3, 57–89.

[9] Kaewchoothong N., Sukato T., Narato P., Nuntadusit C.: *Flow and heat transfer characteristics on thermal performance inside the parallel flow channel with alternative ribs based on photovoltaic/thermal (PV/T) system*. Appl. Therm. Eng. **185**(2021), 116237.

[10] Kaewchoothong N., Maliwan K., Takeishi K., Nuntadusit C.: *Effect of inclined ribs on heat transfer coefficient in stationary square channel*. Theor. Appl. Mech. Lett. **7**(2017), 6, 344–350.

[11] Thapa R.K., Bisht V.S., Bhandari P., Rawat K.S.: *Numerical study of car radiator using dimple roughness and nanofluid*. Arch. Thermodyn. **43**(2022), 3, 125–140.

[12] Chaube A., Sahoo P.K., Solanki S.C.: *Effect of roughness shape on heat transfer and flow friction characteristics of solar air heater with roughened absorber plate*. WIT Trans. Eng. Sci. **53**(2006), 43–51.

[13] Karmare S.V., Tikekar A.N.: *Analysis of fluid flow and heat transfer in a rib grit roughened surface solar air heater using CFD*. Sol. Energy **84**(2010), 3, 409–417.

[14] Rajput R.S., Bhagoria J.L., Giri A.K., Kumar A.: *Study of heat transfer and friction characteristic of various artificial roughness in solar air heater duct by using computational fluid dynamics (CFD) software*. In: Proc. Int. Conf. on Advances in Renewable Energy (ICARE 2010), MANIT Bhopal, June 26-29, 2010, 048.

[15] Chaube A., Sahoo P.K., Solanki, S.C.: *Analysis of heat transfer augmentation and flow characteristics due to rib roughness over absorber plate of a solar air heater*. Renew. Energ. **31**(2006), 317–331.

[16] Yadav A.S., Bhagoria J.L.: *A CFD based thermo-hydraulic performance analysis of an artificially roughened solar air heater having equilateral triangular sectioned rib roughness on the absorber plate*. Int. J. Heat Mass Transf. **70**(2014), 1016–1039.

[17] Semalty A., Bisht V.S., Bhandari P., Rawat K., Singh J., Kumar K., Dixit A.K.: *Thermodynamic investigation on solar air heater having roughness as multiple broken arc and circular protrusion*. Mater. Today: Proc. **69**(2022), 2, 181–186.

[18] Bohra J., Bisht V.S., Bhandari P., Rawat K.S., Singh J., Kumar K., Rawat B.: *Effect of variable blockage height ratio on performance for solar air heater roughened with 45° Z-shaped baffles*. Mater. Today: Proc. **69**(2022), 2, 153–157.

[19] ANSI/ASHRAE Standard 93-2003. Method of Testing to Determine the Thermal Performance of Solar Collectors. American Society of Heating, Refrigeration and Air Conditioning Engineers, Atlanta 2003.

[20] Güler H.Ö., Sözen A., Tuncer A.D., Afshari F., Khanlari A., Şirin C., Gungor A.: *Experimental and CFD survey of indirect solar dryer modified with low-cost iron mesh*. Sol. Energy **197**(2020), 371–384.

[21] Afshari F., Muratçobanoğlu B.: *Thermal analysis of Fe_3O_4/water nanofluid in spiral and serpentine mini channels by using experimental and theoretical models*. Int. J. Environ. Sci. Technol. **20**(2023), 2037–2052.

[22] Afshari F., Ceviz M.A., Mandev E., Yıldız F.: *Effect of heat exchanger base thickness and cooling fan on cooling performance of Air-To-Air thermoelectric refrigerator; experimental and numerical study*. Sustain. Energy Tech. Assess. **52**(2022), 102178.

[23] Bhandari P., Prajapati Y.K.: *Influences of tip clearance on flow and heat transfer characteristics of open type micro pin fin heat sink*. Int. J. Therm. Sci. **179**(2022), 107714.

[24] Kaewchoothong N., Nuntadusit C.: *Flow and heat transfer behaviors in a two-pass rotating channel with rib turbulators using computational fluid dynamics*. Heat Transf. Eng. **44**(2023), 2, 175–195.

[25] Puzu N.O., Prasertsan S., Nuntadusit C.: *Heat transfer enhancement and flow characteristics of vortex generating jet on flat plate with turbulent boundary layer*, Appl. Therm. Eng. **148**(2019), 196–207.

[26] Piya I., Narato P., Wae-hayee M., Nuntadusit C.: *Flow and heat transfer characteristic of inclined oval trench dimples with numerical simulation.* CFD Lett. **12**(2020), 11, 61–71.

[27] Eiamsa-ard S., Nuntadusit C., Promvonge P.: *Effect of twin delta-winged twisted-tape on thermal performance of heat exchanger tube.* Heat Transf. Eng. **34**(2013), 15, 1278–1288.

[28] Webb R.L., Eckert E.R.G.: *Application of rough surface to heat exchanger design.* Int. J. Heat Mass Transf. **15**(1972), 9, 1647–165.

[29] Bhandari P., Prajapati Y.K.: *Fluid flow and heat transfer behavior in distinct array of stepped micro-pin fin heat sink.* J. Enhanc. Heat Transf. **28**(2021), 4, 31–61.

[30] Bhandari P.: *Numerical investigations on the effect of multi-dimensional stepness in open micro pin fin heat sink using single phase liquid fluid flow.* Int. Commun. Heat Mass Transf. **138**(2022), 106392.

[31] Chauhan R., Singh T., Kumar N., Patnaik A., Thakur N.S.: *Experimental investigation and optimization of impinging jet solar thermal collector by Taguchi method.* Appl. Therm. Eng. **116**(2017), 100–109.

[32] Sharma A., Awasthi A., Singh T., Kumar R., Chauhan R.: *Experimental investigation and optimization of potential parameters of discrete V down baffled solar thermal collector using hybrid Taguchi-TOPSIS method.* Appl. Therm. Eng. **209**(2022), 118250.

[33] Chauhan R., Singh T., Thakur N.S., Patnaik A.: *Optimization of parameters in solar thermal collector provided with impinging air jets based upon preference selection index method.* Renew. Energ. **99**(2016), 118–126.

[34] Chauhan R., Kim S.C.: *Thermo-hydraulic characterization and design optimization of dimpled/protruded absorbers in solar heat collectors.* Appl. Therm. Eng. **154**(2019), 217–227.

[35] Chauhan R., Singh T., Patnaik A., Thakur N.S., Kim S.C., Fekete G.: *Experimental investigation and multi objective optimization of thermal-hydraulic performance in a solar heat collector.* Int. J. Therm. Sci. **147**(2020), 106130.

[36] Kumar R., Goel V., Singh P., Saxena A., Kashyap A.S., Rai A.: *Performance evaluation and optimization of solar assisted air heater with discrete multiple arc shaped ribs.* J. Energy Stor. **26**(2019), 100978